



**VICTORIA UNIVERSITY**  
MELBOURNE AUSTRALIA

*Measurements of specific heat capacity of common building materials at elevated temperatures: a comparison of DSC and HDA*

This is the Accepted version of the following publication

Pooley, Lachlan, Abu-Bakar, AS, Cran, Marlene, Wadhwani, Rahul and Moinuddin, Khalid (2019) Measurements of specific heat capacity of common building materials at elevated temperatures: a comparison of DSC and HDA. *Journal of Thermal Analysis and Calorimetry*. ISSN 1388-6150

The publisher's official version can be found at  
<https://link.springer.com/article/10.1007%2Fs10973-019-09124-5>  
Note that access to this version may require subscription.

Downloaded from VU Research Repository <https://vuir.vu.edu.au/40174/>

# Measurements of specific heat capacity of common building materials at elevated temperatures - A comparison of DSC and HDA

Lachlan I. Pooley<sup>1</sup>, Ariza S. Abu-Bakar<sup>2</sup>, Marlene J. Cran<sup>1</sup>, Rahul Wadhvani<sup>1</sup>, Khalid A. M. Moinuddin<sup>1\*</sup>

<sup>1</sup>Institute for Sustainable Industries and Liveable Cities, Victoria University, PO Box 14428, Melbourne, Victoria 8001, Australia;

<sup>2</sup>School of Housing, Building and Planning, Universiti Sains Malaysia, 11800. Penang, Malaysia;

\*Corresponding author: [khalid.moinuddin@vu.edu.au](mailto:khalid.moinuddin@vu.edu.au); Tel.: +61 3 9919 8042

## Abstract

The objective of this study is to investigate how the specific heat capacity ( $c_p$ ) value of a material changes with respect to temperature and heating rate of that material. In-depth knowledge in the variation of  $c_p$  will provide a better knowledge of the thermo-physical properties of these materials and will increase the capabilities and fidelity of computational fluid dynamics (CFD) based fire modelling. The models and simulations are reliant on input data gained through experimentation and this allows for the present study to provide such input data and trends, which are useful in understanding how fires respond in different situations. The value of  $c_p$  in relation to the rate of temperature change has been measured using differential scanning calorimetry (DSC) and hot disk analysis (HDA). This study encapsulates the determination of  $c_p$  values, trends and equations for poly(methyl methacrylate (PMMA), pinewood, pinewood char and two fabrics: cotton and wool. The  $c_p$  values were found to increase with the sample temperature and for two fabrics, they vary with the change in heating rate. The derived equations show that  $c_p$  values from DSC and HDA are comparable. To include these relationships in CFD-based fire models, a set of suggestions have been made.

**Keywords:** DSC; hot disk analyser; specific heat capacity; PMMA; pinewood; fabric

## Nomenclature:

$\beta_s$  Heating rate, K min<sup>-1</sup>

$C$  Specific heat, J g<sup>-1</sup> K<sup>-1</sup>

$c_p$  Specific heat capacity, J g<sup>-1</sup> K<sup>-1</sup>

$c_{p,a}$  Specific heat capacity, J g<sup>-1</sup> K<sup>-1</sup>

$c_r$  Specific heat capacity of reference sample, J g<sup>-1</sup> K<sup>-1</sup>

$\frac{dH}{dt}$  Heat flow to the sample, mW

$\frac{dH_r}{dt}$  Heat flow to the reference material, mW

$H$  Enthalpy, J

$m$  Mass, g

$m_o$  Sample mass, g

40	$m_r$	Reference mass, g
41	$p$	Pressure constant
42	$Q$	Heat flow, J
43	$\Delta Q$	Change in heat flow, mW
44	T	Temperature, °C or K
45	$\Delta T$	Change in temperature, °C or K

## 46 **1 Introduction**

47 Fire models and simulations are much more cost effective in determining important factors that contribute  
 48 to fire behaviour, prevention, suppression and control. Full and medium-scale experimentation in compartment  
 49 fire testing, however, is cost prohibitive. This constraint therefore requires the use of numerical fire modelling  
 50 which needs input parameters from a controlled miniature and/or bench-scale testing environment to gather  
 51 fundamental experimental data. It is imperative that the data from experimental testing and analysis are able to  
 52 validate models of fire behaviour [1]. More accurate predictions of fire can lead to a better understanding of the  
 53 associated fire risk and reliable fire prevention and systems can be implemented to reduce the risk. This is  
 54 economically beneficial for insurers, building owners and clients, who would benefit from a reduction in fire  
 55 damage subsequently reducing the cost of a fire incidence.

56 Poly(methyl methacrylate (PMMA), pinewood, cotton and wool are some common materials that are used  
 57 throughout the building and manufacturing industry. These materials have a wide range of uses and are found  
 58 in diverse environments in which they are typically clustered. In instances where these materials are exposed to  
 59 a fire situation, the surrounding temperature varies as the fire grows or declines and the materials can be heated  
 60 with different heating rates. With regard to the heating rate of the material, the accurate measurement of specific  
 61 heat capacity ( $c_p$ ), among other thermo-physical and flammability parameters, is required for input values for  
 62 computational fluid dynamics (CFD) based fire models such as fire dynamic simulation (FDS) [2] to improve  
 63 fidelity. A variation in heating rate is known to have an effect on the thermo-physical properties of different  
 64 materials [3, 4] and  $c_p$  has an influence on many thermo-physical processes that occur during a fire including  
 65 ignition point, phase change and chemical interactions during pyrolysis. The  $c_p$  value is useful when determining  
 66 regions of thermal activation, volatilization and pyrolysis, therefore, studies are needed to focus on estimating  
 67  $c_p$  of the materials. In CFD based fire simulations, it is crucial that accurate input values are used including  
 68 variations in terms of temperature, heating rate, heat flux etc. [5]. Small scale testing can be used to accurately  
 69 determine the  $c_p$  value of the materials as a prerequisite for simulation but also to verify if these simulations are  
 70 predictive of large fires [6].

71 The  $c_p$  value can be determined using numerous methods with varying degrees of accuracy and sources of  
 72 errors with different calorimetry instruments [7] including the differential scanning calorimeter (DSC) and hot  
 73 disk analyser (HDA) apparatus. These instruments can provide a range of thermo-physical data for a wide range  
 74 of materials and are readily commercially available. The DSC can provide quantitative and qualitative data on  
 75 transitions of materials with temperature, heating rate, degradation environment, and can be used to estimate  
 76  $c_p$ , thermal conductivity ( $k$ ), latent heat, transition temperature and enthalpy [4, 7]. However, the DSC requires  
 77 significant effort in post-processing the raw data to obtain  $c_p$  and  $k$  values. Moreover, the thermal behaviour of  
 78 the material studied is normally compared with a reference material such as sapphire making the process time  
 79 consuming and expensive. The HDA instrument can be used to determine the thermal diffusivity,  $k$  and  $c_p$  and  
 80 its companion software provides these values readily. The primary variance between the two instruments is that  
 81 the DSC gives  $c_p$  as a function of both heating rate and temperature, whereas the HDA provides the data as a

82 function of temperature only. Differential thermal analysis (DTA) is another technique closely related to the  
 83 DSC, however, the DSC can provide greater accuracy and is the preferred method of determining  $c_p$  [8].  
 84 Although literature exists on the effect of temperature on PMMA and various species of pinewood, there are  
 85 few reports of the effect of heating rate on pinewood char, cotton and wool [9]. Goodrich [9] observed that there  
 86 are substantial difficulties with materials of a similar nature to cotton and wool which may account for the lack  
 87 of conclusive research in this particular area.

88 For some materials, especially those undergoing endothermic reactions, heating rates higher than  $5 \text{ K min}^{-1}$   
 89 are recommended for thermal analysis [10] and are considered to be macroscopic heating rates. Therefore, in  
 90 the present study,  $c_p$  was measured as a function of the rate of temperature change for heating rates of 50, 100  
 91 and  $200 \text{ K min}^{-1}$  with these high heating rates likely to occur in building fires. Using DSC measurements, raw  
 92 data was obtained using the sapphire method [11] and  $c_p$  was calculated using post processing in MATLAB.  
 93 Using the same materials, experiments using HDA equipment were performed where the sample was heated in  
 94 an oven until a thermocouple attached to the sample showed that it reached the desired temperature then the  $c_p$   
 95 value was measured at that temperature. The data from both sets of apparatus was used to develop possible  
 96 equations for use in fire engineering applications and also within fire modelling algorithms.

## 97 2 Materials and Methods

### 98 2.1 Concept of Specific Heat Capacity for Determination for using DSC

99  $c_p$  is the amount of thermal energy (J) that is required to change the temperature of 1 g of material by 1 K  
 100 at constant pressure and expressed in  $\text{J g}^{-1} \text{ K}^{-1}$ . Thermodynamically,  $c_p$  is determined by the equation:

$$c_p = \left( \frac{\partial H}{\partial T} \right)_p \quad (1)$$

101 where,  $H$  is enthalpy;  $T$  is temperature of the system;  $p$  is the pressure constant.

102 The derivation of  $c_p$  can also be expressed as:

$$c_p = \frac{\delta Q}{dT} \cdot \frac{1}{m} \quad (2)$$

103 where,  $Q$  is heat;  $m$  is mass. The amount of energy or heat that is exchanged for the change in temperature from  
 104  $T_1$  to  $T_2$  for a given mass  $m$  and specific heat  $c_p(T)$ .

$$Q = m \int_{T_1}^{T_2} c_p(T) dt \quad (3)$$

105 The characteristic equation that is used to determine the  $c_p$  from DSC is:

$$c_p = \frac{\Delta Q}{\Delta T} \quad (4)$$

106 Equation (4) can be utilised using the DSC curves of the heat flow and physical quantity.

107 Taking into account the heating rate,  $c_p$  can be calculated using the following formula:

$$c_p = \frac{1}{m_o \cdot \beta_s} \cdot \frac{dH}{dt} \quad (5)$$

108 where  $\beta_s$  is the heating rate of the sample;  $m_o$  is the sample mass;  $\frac{dH}{dt}$  is the blank curve corrected heat flow to  
 109 the sample. The sample is required to be stable throughout the heating range in order to determine the specific  
 110 heat.

111 Depending on the method used to determine  $c_p$ , if a sample or known reference material is used then  $c_p$  is  
 112 calculated by:

$$c_p = \frac{m_r}{m_o} \cdot \frac{dH/dt}{dH_r/dt} \cdot c_r \quad (6)$$

113 where  $m_r$  is the reference mass;  $c_r$  is the specific heat capacity of the reference mass;  $\frac{dH_r}{dt}$  is the heat flow of  
 114 the reference. The temperature range for this study was selected up to which no thermal degradation (mass loss)  
 115 occurs in order to avoid a mass correction for the evaluation of the  $c_p$ . Thermogravimetric analysis data from a  
 116 previous study [12] and a concurrent study [13] show that PMMA, pine and cotton have minimal mass loss up  
 117 to 300 °C and for wool up to 275 °C. Therefore, only results up to these regions are evaluated.

118 The concept, and experimental technique to obtain HDA data can be found in [5, 12]. It should be noted  
 119 that HDA does not require calibration since the Kraption sensor infused with nickel wire is calibrated by the  
 120 manufacturer. The data affected by the contact sensor resistance lies in the non-linear region at the start of the  
 121 experiment and is thus automatically remove from the calculation of material properties [14]. The following  
 122 sections describe the DSC method for obtaining the  $c_p$ .

## 123 2.2 Obtaining $c_p$ using DSC

### 124 2.2.1 Sample Preparation

125 The samples of PMMA were crushed into small granules approximately 1 mm<sup>2</sup> or smaller. Pinewood dust  
 126 and parings of approximately 0.6-1 mm<sup>2</sup> were used. The cotton and wool samples were cut into small fragments  
 127 ranging between 0.5 and 1.2 mm<sup>2</sup>. Sample masses between 1.3 and 4.2 mg were used to ensure that the DSC  
 128 could obtain a suitable measurement signal. The sample weights also ensured the crucibles were not over filled  
 129 which potentially could have hindered the measurement of heat flow. Aluminium crucibles of 40 µL capacity  
 130 were used in a Mettler Toledo DSC instrument [15]. Weighing errors were minimised with the use of a  
 131 microbalance. Additionally, samples were reweighed when consistency between samples varied. The samples  
 132 were placed in a conditioning unit prior to being encapsulated in the crucibles to reduce the moisture content in  
 133 the materials, and also to verify the affect that moisture content has on materials when determining  $c_p$ . The  
 134 relative humidity of the conditioning unit where the samples were kept was approximately 50% at 23°C.

### 135 2.2.2 Experimental/operating procedure

136 The DSC instrument was fully calibrated by the indium standard prior to sample measurements [16].  
 137 During the measurement, an inert atmosphere was created under a nitrogen flow of 50 mL min<sup>-1</sup>. This represents  
 138 an atmosphere in the absence of air which occurs when during flaming combustion thus preventing air reaching  
 139 the burning material. The sapphire method for  $c_p$  determination was used as this method produces an accuracy  
 140 that is within ± 2% [10, 12]. This method has been experimentally noted to have a variation of ± 5% for the  
 141 value of sapphire material [17].

142 A “baseline” or blank measurement was performed for each heating rate (50, 100 and 200 K min<sup>-1</sup>) in  
 143 order to determine the signal bias in the system. This was obtained by determining the response of both crucibles  
 144 when empty and allows for the signal bias to be removed from the data. A reference test for each heating rate  
 145 was performed to ascertain the difference between the sapphire reference material with well-defined known  
 146 specific heat values and the experimental sample. All of the results obtained were blank curve corrected and  
 147 performed in triplicate.

148 There are two predominant methods of sealing the sample crucibles, namely without lid pinholes [4, 18],  
 149 and with pinhole pierced lids [19]. Rath et al. [20] compared the used of an open pan and one with a lid pinhole  
 150 and found that the presence of the lid effected both the heat flow and exothermic thermal effect of the sample.  
 151 Other studies have also shown the effect of heat rate on samples and also the uncertainty of the results from  
 152 DSC [21, 4, 22]. From these studies, it appears that the pinhole lid has a minimal effect depending on whether

153 gasses are released from the sample during the heating process. The test material and the reference were placed  
 154 into individual aluminium crucibles which were then sealed with pierced lids. The data from the DSC was  
 155 recorded, then analysed using MATLAB in order to obtain the  $c_p$  from the data. Taking into account the  
 156 uncertainty of sample mass, variations between samples and DSC accuracy [21, 23], the standard error was  
 157 estimated to be  $\pm 3\text{-}5\%$ .

### 158 3 Results and Discussion

159 With all four materials, we either observe moisture evaporation or phase transition (such as melting) or  
 160 both. Such physical phenomenon involves enthalpy changes which are not part of the specific heat capacity. In  
 161 literature [24] a combination of the specific heat capacity and additional enthalpy changes are describes as  
 162 "apparent specific heat capacity" and we use  $c_{p,a}$  as the symbol of it. We have plotted "apparent specific heat  
 163 capacity" in Figures 1-7. However, the equations of  $c_p$  were determined from data and trends of the experimental  
 164 data excluding enthalpy changes. The equation type has been selected for fire engineering purposes and CFD-  
 165 based fire modelling simulations. Fire engineering has been emphasized over computer simulations, as fire  
 166 engineers are more reliant on desktop computational methods since they typically do not have access to  
 167 extensive experimental data resources and simulation computation. This has therefore limited the calculations  
 168 to linear and polynomial equations.

#### 169 3.1 PMMA

170 Figure 1 shows the  $c_{p,a}$  of PMMA tested between 25 and 300 °C at different heating rates between 50 and  
 171 200 K min<sup>-1</sup>. However, the data below 70 °C for 200 K min<sup>-1</sup> and 45 °C for 100 K min<sup>-1</sup> are excluded due to  
 172 uncertainty in the initial measurement.  
 173

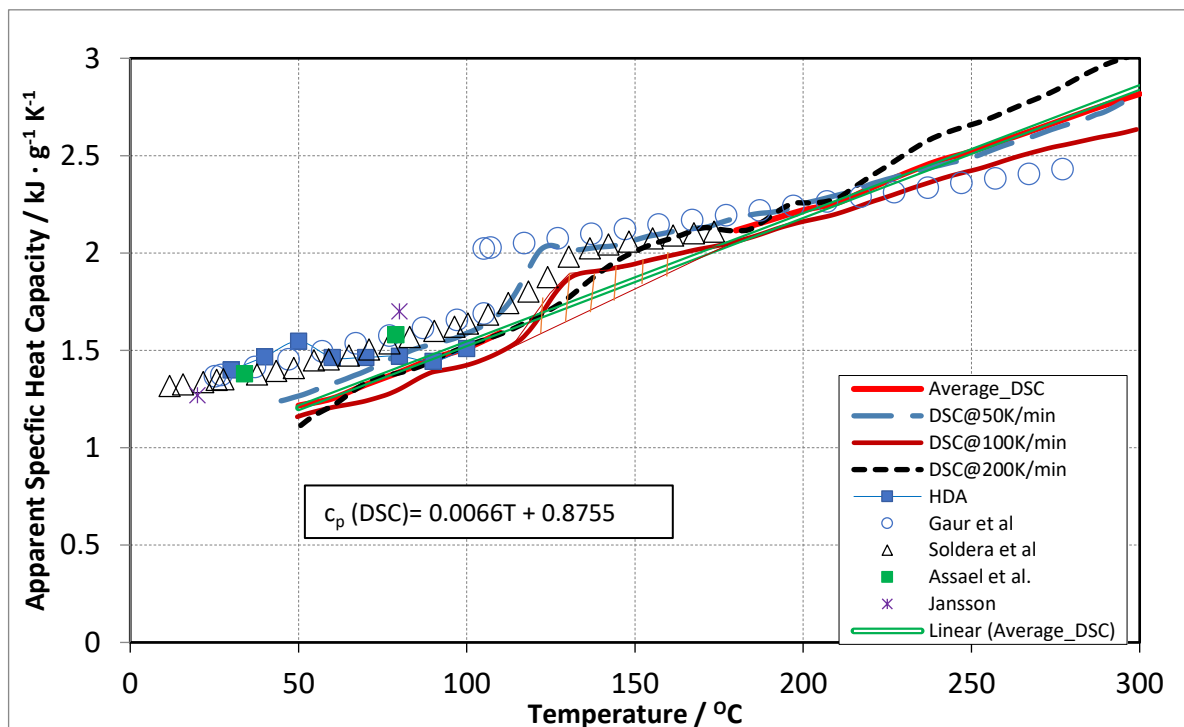


Figure 1. Apparent specific heat capacity variance of PMMA. The hatched pattern shows exemplar phase transition enthalpy as well as the difference between the specific heat capacity and the apparent specific heat capacity.

174

175 It can be observed that between 120 °C and 145 °C there is a peak in all  $c_{p,a}$  - temperature profiles which  
 176 is an indication of transition from a solid state to a melted state. As an example, phase transition enthalpy for  
 177 100 K.min<sup>-1</sup> profile is shown as hatched pattern and this shows the difference between the specific heat capacity  
 178 and the apparent specific heat capacity. This transition was also observed by Gaur et al. [25] and Soldera et al.  
 179 [26] as shown in Figure 1. For this reason, the  $c_p$  values are obtained using HDA up to 100 °C as the equipment  
 180 is only designed to obtain the data from a solid state where no phase change of material or significant  
 181 degradation of material takes place. The  $c_p$  values from HDA are also plotted in Figure 1 and the data between  
 182 two apparatus are markedly comparable. The  $c_p$  values from the DSC (excluding phase transition range) have  
 183 been averaged as the heating rates ranged from 50 to 200 K min<sup>-1</sup> and the averaged profile is presented in Figure  
 184 1. Undertaking a least squares analysis, we obtain a relationship presented as Eq (7), where T is in °C:

$$c_p \text{ (DSC)} = 0.0066 T + 0.8755 \text{ kJ g}^{-1} \text{ K}^{-1} \text{ (r}^2=1.0) \quad (7)$$

185 This equation follows the  $c_p$  profile obtained for 200 K min<sup>-1</sup> prior to melting, after melting the equation  
 186 follows the  $c_p$  profile obtained for 50 K min<sup>-1</sup>. Both HDA data and Eq (7) (averaged  $c_p$  from DSC) are compared  
 187 with other literature studies. Data from Assael et al. [27] and Jansson [28] show linear relationships and their  
 188 values are close to the values obtained in the current study. Prior to and after melting, linear relationships are  
 189 also observed by Gaur et al. [25] and Soldera et al. [26]. Overall literature values are close to those in the current  
 190 study.

### 191 3.2 Pinewood: Virgin and Char

192 Figure 2 and Figure 3 show the  $c_{p,a}$  values of virgin pinewood. A peak bordering 100°C in the HDA data  
 193 represents a moisture affected region with similar peaks more pronounced in the DSC data. At lower heating  
 194 rates, the peaks are higher although they occur over a smaller temperature range. As the water evaporates at 100  
 195 °C, we can assume that these regions are affected by moisture content and its evaporation. Figure 2 shows this  
 196 region affected by evaporation which ends between 170 °C at a heating rate of 50 K min<sup>-1</sup> (moisture evaporation  
 197 enthalpy is shown by hatched pattern) and 217 °C at a heating rate of 200 K min<sup>-1</sup> for the data obtained using  
 198 the DSC. Above these temperatures, the  $c_p$  value increases with temperature.

199 In Figure 3, data beyond the moisture affected region is represented up to 300 °C. The  $c_p$  value changes  
 200 with the rate of heating are apparent within one thermal set, comprising data of 50 to 200 K min<sup>-1</sup>. The values  
 201 in 100 and 200 K min<sup>-1</sup> are close to each other in relative terms and the values of 50 K min<sup>-1</sup> are higher which  
 202 may be due to the effect of thermal transport. The sudden drop at 240 °C for the data obtained at 50 K min<sup>-1</sup> can  
 203 be attributed to pressure from vapour being released from the timber causing the seal and pinhole on the crucible  
 204 lid to widen. This sudden endothermic peak in the data accounts for the shape of the graph.

205 In Figure 3, literature data [29-32] from dry wood is also presented although it should be noted that Gupta  
 206 et al. [29] used a DSC to measure the  $c_p$  at 5 K min<sup>-1</sup> heating rate. Moreover, the literature data [29-31] is only  
 207 reported up to 140 °C, whereas the current study values are extended to 300 °C. From 160 to 300 °C, the  $c_p$   
 208 values from the DSC have been averaged (without endothermic data) with the profile presented in Figure 3 and  
 209 a relationship presented as Eq (8) is obtained undertaking a least squares analysis, where T is in °C:

$$c_p \text{ (DSC)} = 0.004 T + 0.6554 \text{ kJ g}^{-1} \text{ K}^{-1} \text{ (r}^2=0.94) \quad (8)$$

210 Eq (9) can be derived from the HDA data (excluding the data within the moisture affected region) [5],  
 211 where T is in °C:

$$c_p \text{ (HDA)} = -10^{-5} + 0.0057 T + 0.9904 \text{ kJ g}^{-1} \text{ K}^{-1} \text{ (r}^2=0.98) \quad (9)$$

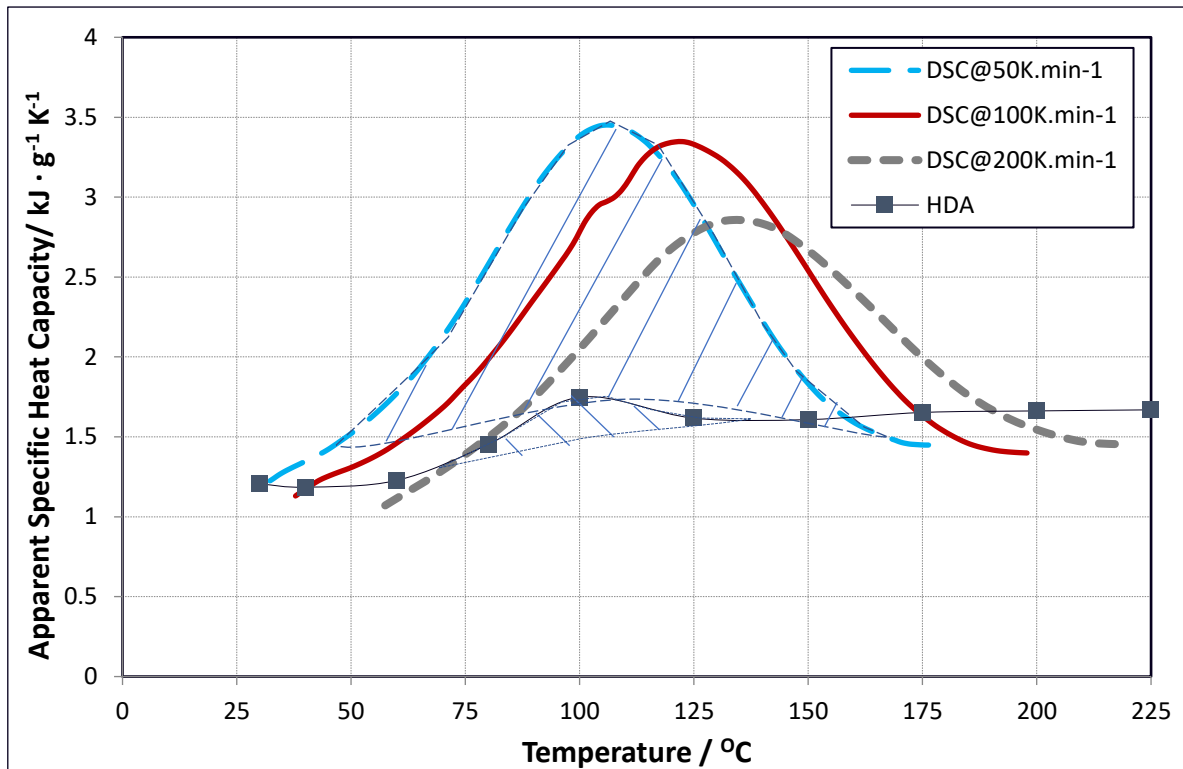


Figure 2. Apparent specific heat capacity variance of pinewood (moisture influenced region). The hatched pattern shows exemplar moisture evaporation enthalpy.

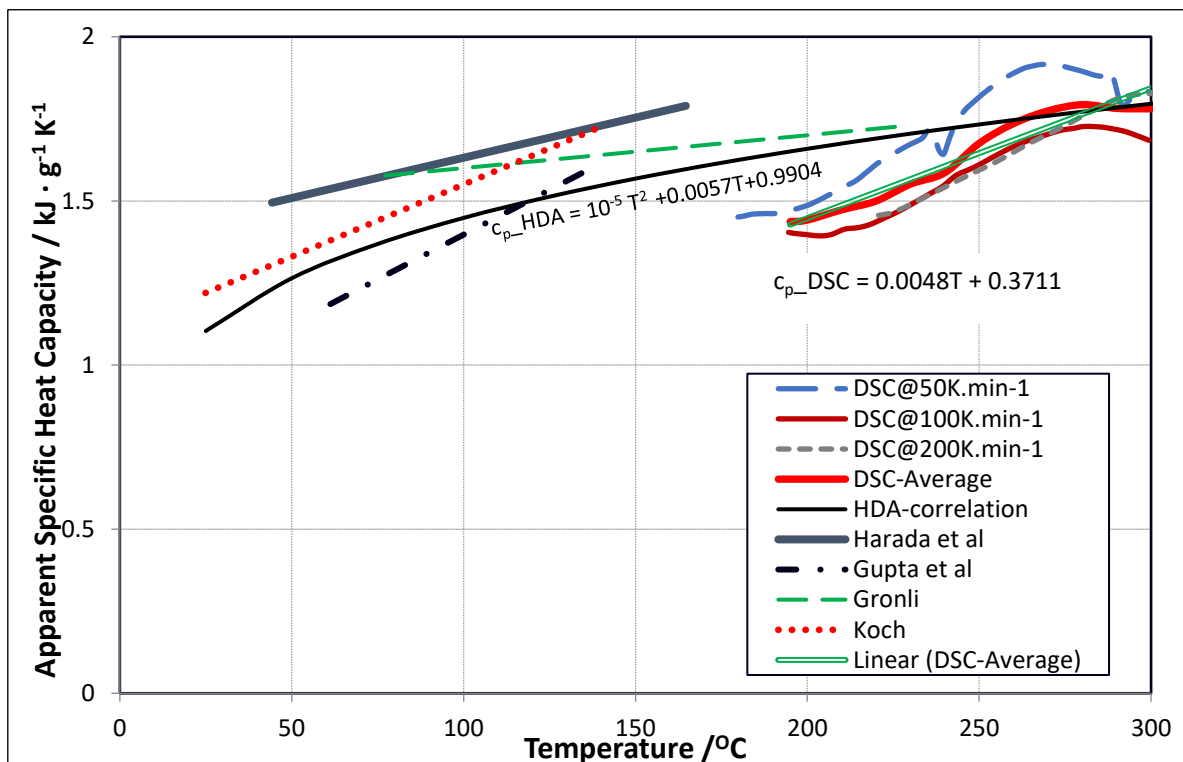


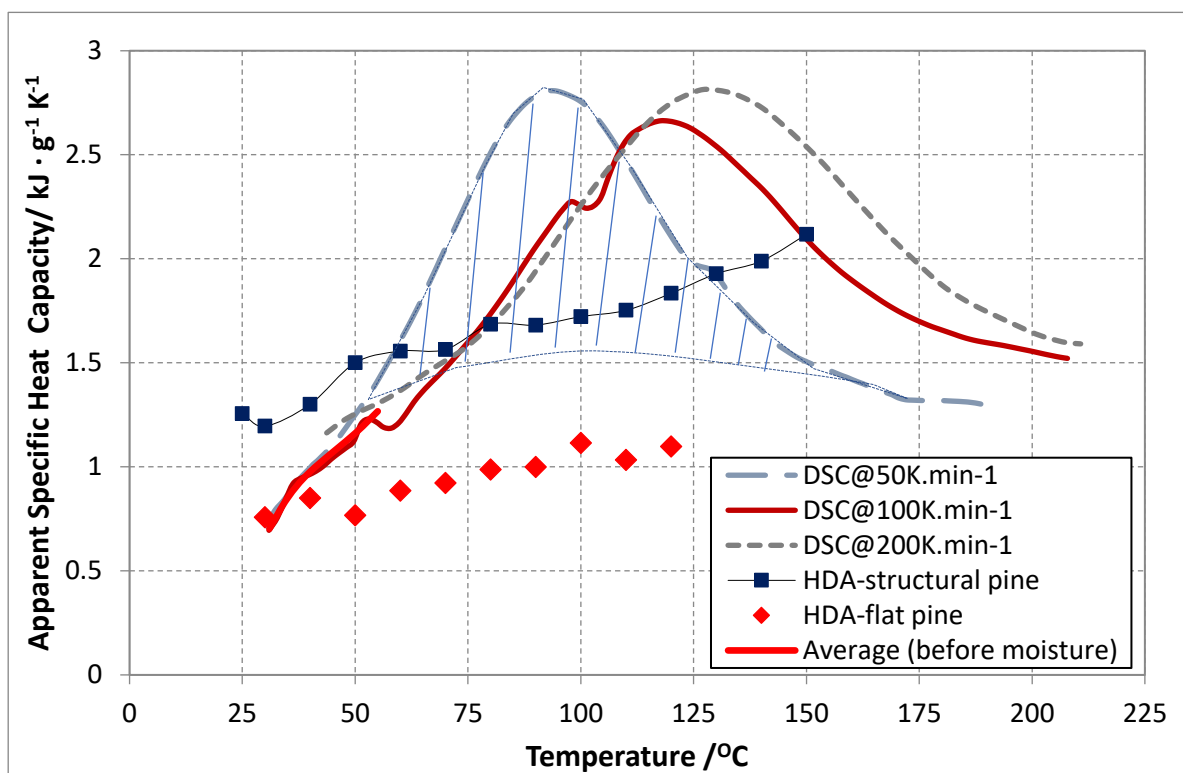
Figure 3. Apparent specific heat capacity without moisture evaporation region of pinewood

212 The DSC data could not be compared with the literature data since up to 170°C, the data is moisture  
 213 affected. Yet, the HDA appears to be comparable with the literature data giving us confidence in our  
 214 experimental procedure. Literature values show similar trends that conform to the current data given different



215 species of timber. They show the values at lower temperature ranges that are not affected by the moisture  
 216 evaporation region and can be attributed to using completely dry wood for experiments. It should be noted that  
 217 a diverse range of timbers exist and that even variation exists within the same species of timber.

218 Figure 4 shows the  $c_{p,a}$  of pinewood char tested where the samples were superfluous from larger scale  
 219 testing. The time taken between testing allowed moisture to penetrate the samples by the time DSC tests were  
 220 conducted and this is observed in the results obtained. The enthalpy change in the moisture affected region can  
 221 be observed in Figure 4 for the DSC experiments. Moisture evaporation enthalpy for 50 K.min<sup>-1</sup> profile, as an  
 222 example, is shown as hatched pattern which can be considered the difference between the specific heat capacity  
 223 and the apparent specific heat capacity. Since the HDA data is not affected by moisture, this data shows an  
 224 overall increase in  $c_p$  with increasing temperature with the data from either side of the moisture region presented  
 225 in Figure 4.



226  
 227 **Figure 4.** Variation of  $c_{p,a}$  (DSC data) and  $c_p$  (HDA data) with temperature for pine char. The hatched pattern  
 228 shows exemplar moisture evaporation enthalpy.

229 Increasing linear relationships with temperature proposed by Gupta et al. [29], Gronli et al. [31] and  
 230 Koufopoulos et al. [33] are presented in Figure 5 along with the current study data (moisture affected DSC data  
 231 are excluded). At the lower end of the temperature range, the data from the aforementioned studies show values  
 232 that are comparable to the HDA data of flat-pine char obtained is more aligned with the literature data. From  
 233 the HDA data, Eq (10-11) was derived [5], where T is in °C:

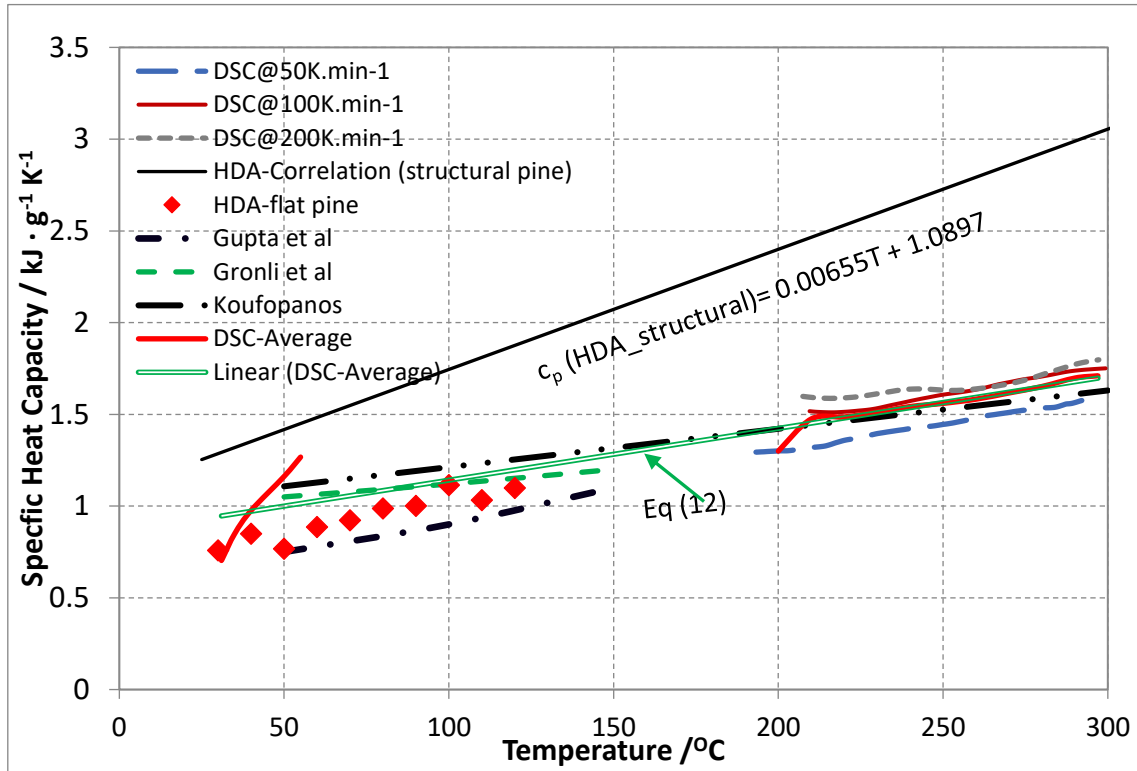
$$\text{Structural pine } c_p \text{ (HDA)} = 0.00655 T + 1.0897 \text{ kJ g}^{-1} \text{ K}^{-1} \text{ (} r^2=0.96 \text{)} \quad (10)$$

$$\text{Flat pine } c_p \text{ (HDA)} = 0.00394 T + 0.6456 \text{ kJ g}^{-1} \text{ K}^{-1} \text{ (} r^2=0.83 \text{)} \quad (11)$$

234 The DSC data shows that between 50 and 200 K min<sup>-1</sup>, the effect of heating rate (thermal transport) on  $c_p$  is not  
 235 significant. The empirical relations that were observed between temperature and  $c_p$  outside the area affected by  
 236 moisture evaporation is presented in Figure 5 with Eq (12) determined:

$$c_p = 0.0028 T + 0.8587 \text{ kJ g}^{-1} \text{ K}^{-1} \quad (r^2=0.88) \quad (12)$$

237 Extrapolation of the data obtained by Koufopoulos et al. [33] and Gupta et al. [29] shows consistency with the  
 238 DSC data of the present study. In this case, the data of Koufopoulos et al. [33] runs almost equivalent with Eq  
 239 (12).



240

241

Figure 5. Variation in  $c_p$  for pinewood char excluding the moisture affected region

### 242 3.3 Cotton and Wool Fabrics

243 Figure 6 shows variation in the  $c_{p,a}$  for cotton and similar to pinewood, the moisture content results in  
 244 enthalpy change in the vicinity of 100°C. The region of moisture evaporation can be observed in Figure 6,  
 245 though this is a subtle representation. The sudden spike in  $c_p$  values observed at around 260 °C for all heating  
 246 rates can be attributed to the phase transition occurring in the cellulose structures within the cotton [34]. In all  
 247 cases this is a significant but not unexpected spike since the cellulose content of cotton is around 90% [35]. As  
 248 an example, moisture evaporation and phase transition enthalpy for 50 K.min<sup>-1</sup> profile are shown as hatched  
 249 patterns and these show the difference between the specific heat capacity and the apparent specific heat capacity.

250 The HDA data is also plotted in Figure 6 and a steadily increasing trend in the  $c_p$  is observed after the  
 251 moisture evaporation region (hatched pattern) was removed. The HDA data generally conforms to the same  
 252 characteristic trend present for the DSC with  $c_p$  values that are comparable. Literature value for cotton from  
 253 Harris [36] at lower temperature is presented in Figure 6 which falls slightly above the range of the DSC values,  
 254 but below HDA, for values at the lowest temperatures presented.

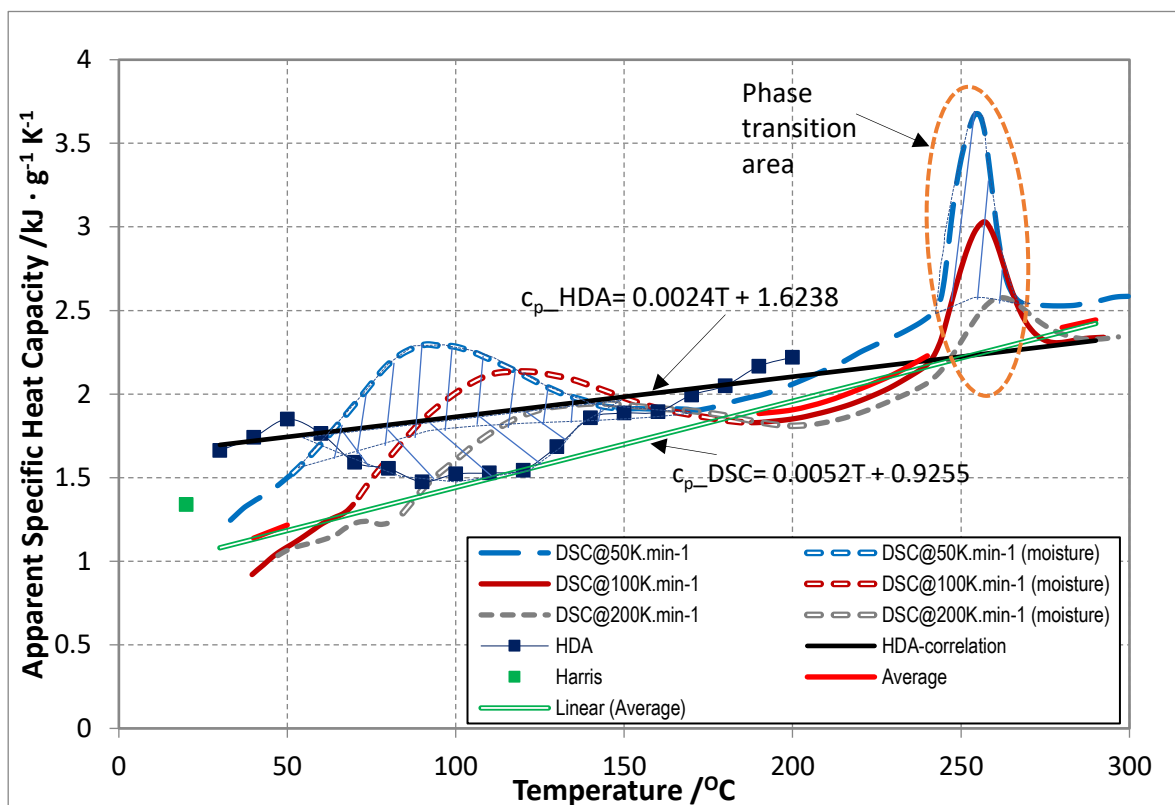
255 To obtain a quantitative trend, the data related to the moisture evaporation and phase transition regions  
 256 were removed. Then, from 40 to 290 °C, the  $c_p$  values from the DSC have been averaged for the heating rates

257 50 to 200 K min<sup>-1</sup>. It can be observed the  $c_p$ -temperature profiles from these three heating rates are close to  
 258 each other implying that the effect of thermal transport is not significant. This averaged profile is also presented  
 259 in Figure 6 and Eq (13) [where T is in °C] was obtained by a least square's regression analysis:

$$c_p (\text{DSC}) = 0.0052 T + 0.9255 \text{ kJ g}^{-1} \text{ K}^{-1} \quad (r^2=0.99) \quad (13)$$

260 Similarly, Eq (14) was derived from the HDA data [5] where T is in °C:

$$c_p (\text{HDA}) = 0.0024 T + 1.6238 \text{ kJ g}^{-1} \text{ K}^{-1} \quad (r^2=0.78) \quad (14)$$



261  
 262 Figure 6. Variation of apparent specific heat capacity for cotton. The hatched pattern shows exemplar  
 263 moisture evaporation and phase transition enthalpy as well as the difference between the specific heat  
 264 capacity and the apparent specific heat capacity.

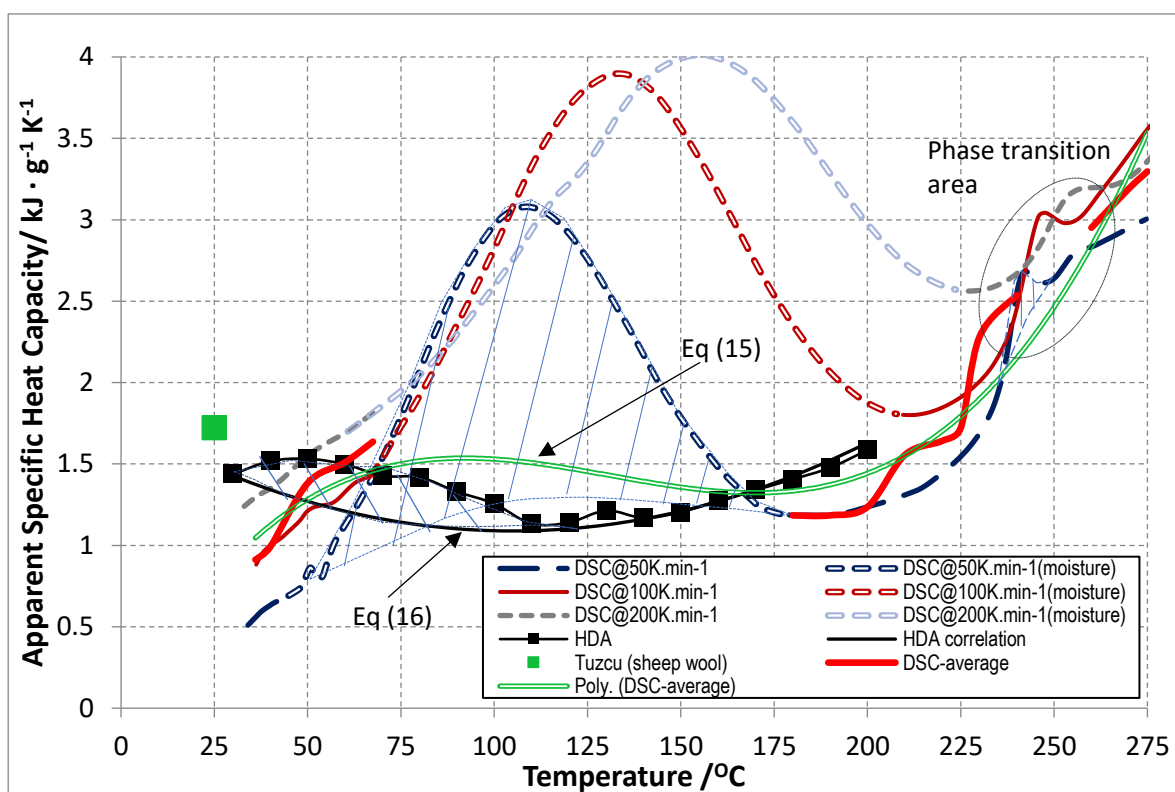
265 Figure 7 shows the variation of  $c_{p,a}$  for wool tested using both the DSC and HDA apparatus, though HDA  
 266 experiments were not conducted beyond 200 °C. Wool is affected by moisture evaporation in the same manner  
 267 as cotton and pinewood. Both the DSC and HDA data shows that shortly after the initiation of heating, the  
 268 moisture affected region is apparent. Phase transition regions are observed in the DSC data which can be  
 269 attributed to the decomposition within the fibres of wool or swelling decrystallisation of various types of amino  
 270 acids present in wool [30, 31]. This can also contribute to the secondary peak and linear increase observed as  
 271 the acids break down into base constituents above the temperature of 225 °C [37, 38]. Similar to cotton data  
 272 presentation in Figure 6, the moisture evaporation and phase transition enthalpy for 50 K.min<sup>-1</sup> profile are shown  
 273 as hatched patterns.

274 To obtain a quantitative trend, all DSC data were analysed excluding the moisture evaporation and phase  
 275 transition. The DSC obtained  $c_p$  values were averaged over all three heating rates data in three regions: (i) from  
 276 25 to 68 °C, (ii) from 180 to 240 °C, and (iii) from 260 to 275 °C. Undertaking a least squares analysis of the  
 277 average profile, the relationship obtained is presented in Eq (15) for the DSC data and in Eq (16) for the HDA  
 278 data [5], where T is in °C:

$$c_p (\text{DSC}) = 9 \times 10^{-7} \times T^3 - 0.000355 T^2 + 0.04237 T - 0.06137 \text{ kJ g}^{-1} \text{ K}^{-1} \quad (r^2=0.94) \quad (15)$$

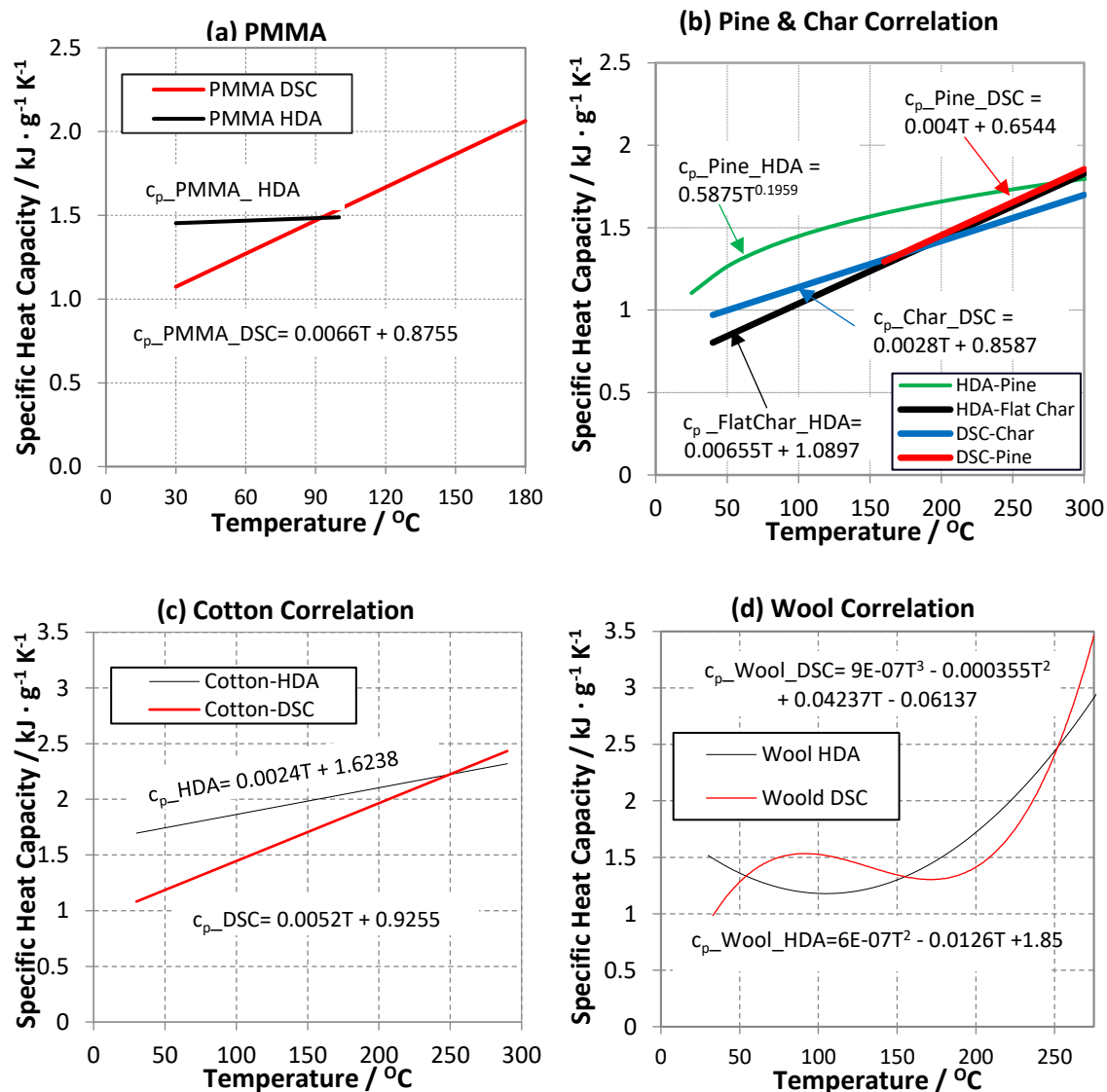
$$c_p (\text{HDA}) = 6 \times 10^{-5} \times T^2 - 0.0126 T + 1.85 \text{ kJ g}^{-1} \text{ K}^{-1} \quad (r^2=0.91) \quad (16)$$

279 In general, the data from both test apparatus are comparable except at low temperatures. Figure 7 also  
 280 presents a comparative literature value for sheep wool as reported by Tuzcu [39] which is slightly higher than  
 281 the values from the current study although it should be noted that this literature data did not take into account  
 282 temperature or heating rate. It can be observed that while the heating rate is varied, before and after the moisture  
 283 evaporation region (until the phase transition occurs),  $c_p$  values differ considerably implying significant effect  
 284 of thermal transport.



285  
 286 Figure 7. Variation of apparent specific heat capacity for wool. The hatched pattern shows exemplar moisture  
 287 evaporation and phase transition enthalpy as well as the difference between the specific heat capacity and the  
 288 apparent specific heat capacity.

289 A summary of the correlations developed for the tested materials is presented in Figure 8 and in general,  
 290 it can be observed that as the temperature increases there is an increase in the  $c_p$  values. As shown, the difference  
 291 between HDA and DSC measurements are not substantial. For each material, at a specific temperature, the  
 292 values intersect and moving away from this intersection point, the difference increases. The maximum  
 293 difference ranges for PMMA, pine, pine char, cotton and wool are  $\pm 0.6$ ,  $\pm 0.3$ ,  $\pm 0.2$ ,  $\pm 0.6$  and  $\pm 0.7 \text{ kJ kg}^{-1} \text{ K}^{-1}$ .  
 294 In the supplementary material, a method is recommended to enable the optimized use of the data.



295 Figure 8. Correlations of  $c_p$  for (a) PMMA, (b) pinewood, virgin and char, (c) cotton, and (d) wool with  
 296 temperature

#### 297 4 Conclusions

298 The  $c_p$  values of common building materials tested with DSC and HDA apparatus are presented in this  
 299 study with their trends determined with respect to temperature. The primary objective is to use the obtained  $c_p$   
 300 values in CFD-based fire simulations for fire engineering and research purposes. While the HDA measurement  
 301 did not involve any heating rate, DSC measurements were conducted at heating rates of 50, 100 and 200 K min<sup>-1</sup>  
 302 as these are likely to occur in substantial fires. DSC materials were roughly measured over a temperature range  
 303 of 25 to 300 °C except for wool up to 275 °C. HDA measurements were conducted from 30 to 100 °C for  
 304 PMMA, 30 to 225 °C pinewood, 25 to 150 °C for char and 30 to 200 °C for cotton and wool.

305 Of all the materials tested, PMMA was the only material not affected by moisture content and PMMA,  
 306 cotton and wool all showed phase transitions at ~125°C, ~260°C and ~245°C respectively. For similar materials,  
 307 literature data was generally comparable to the data obtained in the current study data although typically at  
 308 lower temperatures. This further supports the results obtained at higher temperatures and at different heating  
 309 rate in the current study.

310 The DSC measurements of  $c_p$  values did not change significantly for PMMA and pine char between  
311 heating rates adopted in this study. For pine and cotton slight decrease as heating rate increased are observed.  
312 On the other hand, for wool  $c_p$  values considerably increased as heating rate increased. The effect of thermal  
313 transport varies due to chemical composition, physical and structural properties. It is also noted that the  
314 materials have different fibrous and cellulose structures.

315 Analysis of the DSC and HDA  $c_p$  values for the various materials studied enabled the development of  
316 empirical relationships. The relationships were developed from regions where phase changes were not  
317 occurring, and regions not affected by moisture evaporation. The relationships show that the difference between  
318 HDA and DSC are not substantial. These relationships can be used as input values for CFD-based fire  
319 simulations and models and all materials except for wool showed a linear increase of  $c_p$  values with increasing  
320 temperature. A second and third order curvilinear increase were observed for the  $c_p$  values with HDA and DSC  
321 measurement for wool. Some suggestions are made, in the supplementary material, for how to include these  
322 relationships in CFD-based fire models. The enhanced accuracy of the data will assist in providing higher  
323 fidelity simulations of fire scenarios which can be utilised in order to develop improved designs for reducing  
324 fire risk.

#### 325 **Funding:**

326 This study was conducted through internal funding from Victoria University.

#### 327 **Conflicts of Interest:**

328 The authors report no conflict of interest in this study.

329

#### 330 **References**

- 331 1. Drysdale D. An introduction to fire dynamics. John Wiley & Sons; 2011.
- 332 2. McGrattan K, McDermott R, Weinschenk C, Overholt K, Hostikka S, Floyd J. Fire dynamics simulator (Sixth  
333 Edition) user's guide. Gaithersburg, Maryland, USA: National Institute of Standards and Technology 2015.
- 334 3. Abu-Bakar A, Moinuddin K, editors. Effects of variation in heating rate, sample mass and nitrogen flow on  
335 chemical kinetics for pyrolysis. 18th Australasian fluid mechanics conference Launceston, Australia; 2012;  
336 Launceston, TAS.
- 337 4. Kousksou T, Jamil A, El Omari K, Zeraoui Y, Le Guer Y. Effect of heating rate and sample geometry on  
338 the apparent specific heat capacity: DSC applications. *Thermochimica acta*. 2011;519(1-2):59-64.
- 339 5. Abu-Bakar AS. Characterization of Fire Properties for Coupled Pyrolysis and Combustion Simulation and  
340 Their Optimised Use [PhD]. College of Engineering and Science: Victoria University; 2015.
- 341 6. Linteris GT, Gewuerz L, McGrattan KB, Forney GP. Modeling solid sample burning with FDS. National  
342 Institute of Standards and Technology, NISTIR. 2004;7178:36.
- 343 7. Czichos H, Saito T, Smith LE. Springer Handbook of Materials Measurement Methods. Spring  
344 Science+Business Media; 2007.
- 345 8. Mettler-Toledo. Heat capacity determination at high temperatures by TGA/DSC Part 1: DSC standard  
346 procedures. Schwerzenbach, Switzerland 2010.
- 347 9. Goodrich TW. Thermophysical properties and microstructural changes of composite materials at elevated  
348 temperature: Virginia Tech; 2009.

- 349 10. Kodur VKR, Harmathy TZ. Properties of Building Materials. In: DiNunno PJ, Drysdale D, Beyler CL,  
350 Walton WD, Custer RLP, Hall JR, Jr. et al., editors. SFPE Handbook of Fire Protection Engineering. Third ed.:  
351 National Fire Protection Association; 2002. p. 155-81.
- 352 11. Hohne GWH, Hemminger WF, Flammersheim HJ. Differential Scanning Calorimetry. Springer-Verlag  
353 Berlin Heidelberg New York; 2003.
- 354 12. Abu Bakar AS, Cran M, Moinuddin KAM. Experimental investigation of effects of variation in heating rate,  
355 temperature and heat flux on fire properties of a non-charring polymer. Journal of Thermal Analysis and  
356 Calorimetry. 2019;137(2):447-59. doi:DOI: 10.1007/s10973-018-7941-0.
- 357 13. Abu Bakar AS, Cran M, Wadhvani R, Moinuddin KAM. Characterisation of pyrolysis and combustion  
358 parameters of charring materials most frequently found in buildings Journal of Thermal Analysis and  
359 Calorimetry. 2019;(in Press).
- 360 14. Thermtest I, inventor Thermtest Inc, assignee. Hot Disk Thermal Constants Analyser Instruction Manual.  
361 Canada2012.
- 362 15. Mettler T, inventor DSC1 User's Manual. Switzerland2011.
- 363 16. Mettler-Toledo. DSC Calibration, Temperature and Heat Flow. Mettler-Toledo, Switzerland. 2018.  
364 [https://www.mt.com/au/en/home/supportive\\_content/matchar\\_apps/MatChar\\_HB805.html](https://www.mt.com/au/en/home/supportive_content/matchar_apps/MatChar_HB805.html). Accessed 14  
365 October 2018.
- 366 17. Shaw T, Carrol J. Application of baseline correction techniques to the “ratio method” of DSC specific heat  
367 determination. International journal of thermophysics. 1998;19(6):1671-80.
- 368 18. Milosavljevic I, Oja V, Suuberg EM. Thermal effects in cellulose pyrolysis: relationship to char formation  
369 processes. Industrial & Engineering Chemistry Research. 1996;35(3):653-62.
- 370 19. Shalaev EY, Steponkus PL. Correction of the sample weight in hermetically sealed DSC pans.  
371 Thermochemica acta. 2000;345(2):141-3.
- 372 20. Rath J, Wolffinger MG, Steiner G, Krammer G, Barontini FC, Cozzani V. Heat of Wood Pyrolysis. Fuel.  
373 2003;82(1):81-91.
- 374 21. Rudtsch S. Uncertainty of heat capacity measurements with differential scanning calorimeters.  
375 Thermochemica Acta. 2002;382(1-2):17-25.
- 376 22. Strezov V, Patterson M, Zyma V, Fisher K, Evans TJ, Nelson PF. Fundamental aspects of biomass  
377 carbonisation. Journal of analytical and applied pyrolysis. 2007;79(1-2):91-100.
- 378 23. Dieck RH. Measurement uncertainty: methods and applications. ISA; 2007.
- 379 24. Höhne G, Hemminger WF, Flammersheim H-J. Differential scanning calorimetry. Springer Science &  
380 Business Media; 2013.
- 381 25. Gaur U, Lau Sf, Wunderlich BB, Wunderlich B. Heat capacity and other thermodynamic properties of linear  
382 macromolecules VI. Acrylic polymers. Journal of Physical and Chemical Reference Data. 1982;11(4):1065-89.
- 383 26. Soldera A, Metatla N, Beaudoin A, Said S, Grohens Y. Heat capacities of both PMMA stereomers:  
384 Comparison between atomistic simulation and experimental data. Polymer. 2010;51(9):2106-11.
- 385 27. Assael MJ, Botsios S, Gialou K, Metaxa IN. Thermal Conductivity of Polymethyl Methacrylate (PMMA)  
386 and Borosilicate Crown Glass BK7. International Journal of Thermophysics. 2005;26(5):1595-605.  
387 doi:10.1007/s10765-005-8106-5.
- 388 28. Jansson R. Measurement of thermal properties at elevated temperatures - Brandforsk Project 328-031. SP  
389 Report 2004:46; 2004.
- 390 29. Gupta M, Yang J, Roy C. Specific heat and thermal conductivity of softwood bark and softwood char  
391 particles☆. Fuel. 2003;82(8):919-27.

- 392 30. Harada T, Hata T, Ishihara S. Thermal constants of wood during the heating process measured with the laser  
393 flash method. *Journal of wood science*. 1998;44(6):425-31.
- 394 31. Gronli MG, Antal J, Varhegyi G. A Round-Robin Study of Cellulose Pyrolysis Kinetics by  
395 Thermogravimetry. *Industrial & Engineering Chemistry Research*, 38(6). 1999:2238–44.
- 396 32. Koch P. Specific heat of oven-dry spruce pine wood and bark. *Wood Science Vol 1 (4)*: 203-214. 1968.
- 397 33. Koufopoulos C, Lucchesi A, Maschio G. Kinetic modelling of the pyrolysis of biomass and biomass  
398 components. *The Canadian Journal of Chemical Engineering*. 1989;67(1):75-84.
- 399 34. Ayeni N, Adeniyi A, Abdullahi N, Bernard E, Ogunleye A. Thermogravimetric and kinetic study of  
400 methylolmelamine phosphate treated-cotton fabric. *Bayero Journal of Pure and Applied Sciences*.  
401 2012;5(2):51–5.
- 402 35. Meilert K, Laub D, Kiwi J. Photocatalytic self-cleaning of modified cotton textiles by TiO<sub>2</sub> clusters attached  
403 by chemical spacers. *Journal of molecular catalysis A: chemical*. 2005;237(1-2):101-8.
- 404 36. Harris vM. *Handbook of Textile Fibers*. Harris Research Laboratories, Washington.; 1954.
- 405 37. Horrocks AR, Price D. *Fire Retardent Materials*. Abington Cambridge: Woodhead Publishing Limited;  
406 2001.
- 407 38. Bras ML, Camino G, Bourbigot S, Delobel R. *Fire Retardancy of Polymers: The Use of Intumescence*.  
408 Cambridge: The Royal Society of Chemistry; 1998.
- 409 39. Tuzcu T. *Hygro-thermal properties of sheep wool insulation*: Delft University of Technology; 2007.
- 410